Buried Wireless Sensor Network for Monitoring Pipeline Joint Leakage Caused by Large Ground Movements

Tzu-Hsuan Lin, Ph.D.[1]; Yan Wu, Ph.D.[2]; Kenichi Soga, Ph.D., M.ASCE[3]; Brad Parker Wham, Ph.D., A.M.ASCE[4]; Chalermpat Pariya-Ekkasut, Ph.D.[5]; Blake Berger[6]; and Thomas D. O'Rourke, Ph.D., Dist.M.ASCE[7]

Abstract: This paper proposes an innovative buried wireless sensor network (B-WSN) system for detecting leakage from pipeline joints caused by large ground movements such as earthquakes. The key challenge to any such system is that electromagnetic (EM) signal strength becomes significantly attenuated over short distances when wireless devices are buried in certain materials—notably soil, this paper's focus. After simulation results indicated that the EM radio frequency was a key factor influencing the depth through which a signal can propagate in soil, the B-WSN system was developed, which includes a high-performance sub-1-GHz transceiver that utilizes a low-power band frequency at 433 MHz. Field testing indicated that the BWSN can achieve a penetration depth of 2.13 m. The system configuration includes a radio link budget of 120 dB, transmit power of 26 dBm, receive sensitivity of −125 dBm, and omnidirectional antenna gain of 1.5 dBi. The system works on multihop topology, meaning that each sensing node also acts as a relay node to assist other nodes buried deeper in the ground with data communication. For purposes of this paper, four hops were used, and this made wireless communication possible at an overall burial depth of 8 m. As such, the proposed B-WSN system would be compatible with most buried utility pipelines. The conducted full-scale pipeline-rupture experiment results further verified that the system can, in close to real time, pinpoint locations and subsequent patterns of water leakage caused by severe ground deformation. The findings also exemplify how the B-WSN system could aid structural evaluation of pipelines that are likely to experience large ground deformation. The average packet-loss rate was less than 0.1% during the experiment, and in terms of average power consumption, each sensing node used less than 26.5 mA per 30 s data-reporting period. Thus, the sensing nodes can be expected to function continuously for 27 days if powered by four standard industrial D-cell batteries, or for more than 2 years if the data-reporting period is changed to 1 h. **DOI: 10.1061/(ASCE)PS.1949-1204.0000392.**

Introduction

The pipeline industry has recently introduced innovative segmental pipelines for water distribution and wastewater networks that can offer sizeable joint extension, compression, and rotation to accommodate earthquake-induced ground movements such as fault rupture, liquefaction-induced lateral spreads, and landslides (Wham et al. 2017a, b). Despite such advancements, significant ground-rupture events can result in pipeline damage, and the ability to monitor joint leakage using low-cost sensing technology is advantageous. When many sensors are adopted, wireless communication is particularly favorable because wired sensor systems can be limited by cost or complexity constraints. Smart sensor–based wireless sensor networks (WSNs) are attractive for monitoring joint leakage because of their low manufacturing costs, low power requirements, small size, and simplicity of deployment.

Increasingly, wireless sensors are being proposed for monitoring the performance of pipeline systems. Stoianov et al.'s (2007) PipeNet system is capable of high-sampling-rate sensing for pipeline monitoring. It offers a range of WSN clusters with various sensors and sampling intervals, and its performance has been verified through lab experiments and field testing. It is based, however, on the Bluetooth-dependent Intel Mote platform, and because Bluetooth is not suitable for underground applications, PipeNet must rely on antennae that are extended above the surface of the ground. Yu and Guo (2012) developed a wireless monitoring system for oil and gas pipelines using an efficient pipeline-state information-collection algorithm. They also proposed a three-tiered network architecture for pipeline data collection to optimize the network architecture and algorithm. Similar work on the architecture and protocols of pipeline-based WSNs (Ali et al. 2015;

[1]Assistant Professor, Dept. of Civil Engineering, National Central Univ., Zhongda Rd., Zhongli District, Taoyuan, Taiwan 32001, ROC (corresponding author). ORCID: https://orcid.org/0000-0001-7833-5394. Email: cornetlin@gmail.com

[2]Chief Technology Officer, Wisen Innovation Ltd., Office D501, 530 Mansion, Taihu International Hi-tech Zone, Xinwu District, Wuxi 214135, China. Email: wuyan@wisencn.com

[3]Chancellor's Professor, Dept. of Civil and Environmental Engineering, Univ. of California, Berkeley, CA 94720. Email: soga@berkeley.edu

[4]Assistant Research Professor, Dept. of Civil, Environmental, and Architectural Engineering, Univ. of Colorado Boulder, 1111, Engineering Dr., UCB 428, ECOT 441, Boulder, CO 80309. Email: Brad.Wham@colorado.edu

[5]Instructor, Engineering Military School, Corps of Engineers, Royal Thai Army Univ., Mueang Ratchaburi, Ratchaburi 70000, Thailand. Email: cp494@cornell.edu

[6]Engineer, Thornton Tomasetti, 51 Madison Ave., New York, NY 10010. Email: BBerger@thorntontomasetti.com

[7]Thomas R. Briggs Professor, Geotechnical Lifelines Group, School of Civil and Environmental Engineering, Cornell Univ., B02 Thurston Hall, 130 Hollister Dr., Ithaca, NY 14853. Email: tdo1@cornell.edu

Note. This manuscript was submitted on March 16, 2018; approved on January 7, 2019No Epub Date. Discussion period open until 0, 0; separate discussions must be submitted for individual papers. This paper is part of the ***Journal of Pipeline Systems Engineering and Practice***, © ASCE, ISSN 1949-1190.

Jawhar et al. 2008, 2007) has involved specific site types where aerial communication is possible, such as manholes.

For long-distance water-pipeline leakage detection, Almazyad et al. (2014) proposed a moveable, non-real-time WSN system of sensing nodes that move with the water flow inside a pipeline while collecting data. At any given time, the nodes are located by reading radio frequency identification (RFID) tags that are placed in fixed positions along the outer pipeline surface. Experimental validation of the proposed system, however, was limited. Lai et al. (2012) proposed a pipeline-monitoring system called TriopusNet that automatically deployed and replaced sensors on the inner surface of pipes using three arms driven by a single motor. Its effectiveness was limited because it used a 2.4-GHz radio in a water medium that absorbs radio waves, thereby restricting its transmission range.

Compared with the aforementioned other types of WSN-based pipeline-monitoring systems, buried systems are much more challenging to deploy in the field because of the significant attenuation of electromagnetic (EM) waves in soils. Several studies have addressed radio propagation in below-ground conditions (Akyildiz et al. 2009; Silva and Vuran 2010a). Akyildiz et al. (2009) provided an excellent review of the methods for predicting path losses in underground link applications, and Vuran and Silva (2010) reported on parameters critical to buried wireless sensor networks (B-WSN), such as burial depth, reflection, refraction, and multipath fading effects on EM waves.

To tackle the propagation issue, Sun et al. (2011) proposed a magnetic induction (MI)-based WSN system called MISE-PIPE for underground pipeline monitoring. The system's clustered architecture–based WSN consists of two main parts: a hub layer and an in-soil sensor layer. The nodes in the hub layer are deployed at checkpoints to monitor the pipeline continuously, and the sensors in the in-soil sensor layer are densely deployed along the pipeline to provide more accurate leakage detection and localization results without continuous sensing. Tan et al. (2015) tried to establish MI underground communication and to evaluate its performance in a small-scale testbed by measuring essential characteristics, such as path loss, bandwidth, and packet error rate (PER). However, they were unable to demonstrate its effectiveness in either sensing pipeline leakage or transmitting leakage data. Provided that lower-frequency EM waves (e.g., sub-gigahertz) can achieve sufficiently deep penetration for shallow underground wireless communication, it would be better to use EM waves than MI in cases where the transmission of large amounts of data are needed. Based on experiments with 433 MHz Mica2 motes, Silva and Vuran (2010b) and Yu et al. (2017) found that the maximum penetration depth of underground wireless sensing was 1 m. The Mica2 mote is now outdated, and new technology for sub-gigahertz wireless communication (like LoRa) has been developed.

Few researchers have addressed the problem of using B-WSN for monitoring pipeline joint leakage caused by large ground movements. To the best of the authors' knowledge, no studies have addressed the effectiveness of B-WSNs at detecting joint leakage. Moreover, it is not clear whether leakage can affect wireless propagation or if vast ground movements have an adverse impact on buried wireless nodes. Moreover, there remains a need for an efficient method to estimate an appropriate burial depth before the wireless sensing node is installed.

The present study focuses on developing and investigating the effectiveness of B-WSN for monitoring pipeline joint leakage caused by large ground movements. The proposed system's maximum simulated and actual penetration through soil was first evaluated in the field. Then, a series of soil-moisture sensors were employed during a full-scale fault rupture experiment to assess network performance along a buried pipeline.

Determining the Key Factors Affecting How Far a Signal Propagates through Soil

Extensive theoretical analysis of in-soil signal propagation has been published previously (Akyildiz and Stuntebeck 2006; Akyildiz et al. 2009; Silva and Vuran 2010a; Vuran and Silva 2010), and it commonly uses an EM path-loss model in free space (Akyildiz et al. 2009) to characterize loss, L_0, as follows:

$$L_0 = 20\log\frac{4\pi d}{\lambda_0} = -147.6 + 20\log(d) + 20\log(f) \quad (1)$$

where d = distance between the transmitter and the receiver (m); λ_0 = wavelength in free space; and f $(=1/\lambda_0)$ = operating frequency (Hz).

When an EM wave propagates in the soil, however, the path loss, L_s, has two additional components

$$L_s = L_\beta + L_\alpha \quad (2)$$

where L_β = attenuation loss due to the difference between the wavelength of the signal in the soil, λ, and the wavelength in free space, λ_0; and L_α = transmission loss caused by attenuation. L_β and L_α can be represented in decibels as follows (Akyildiz and Stuntebeck 2006; Akyildiz et al. 2009; Vuran and Silva 2010)

$$L_\beta = 154 - 20\log(f) + 20\log(\beta); \quad L_\alpha = 8.69\alpha d \quad (3)$$

where β = phase-shifting constant (radian/m); and α = attenuation constant (1/m).

By combining Eqs. (1)–(3), the path loss of an EM wave in the soil can be computed as follows:

$$L_p = L_0 + L_s = 6.4 + 20\log(d) + 20\log(\beta) + 8.69\alpha d \quad (4)$$

The attenuation constant α and phase-shift constant β (i.e., $\gamma = \alpha + j\beta$) in Eq. (4) are derived using the Peplinski principle (Peplinski et al. 1995), which governs the value of the complex propagation constant of the EM wave in the soil with the following relationship:

$$\alpha = \omega\sqrt{\frac{\mu\varepsilon'\varepsilon_0}{2}\left[\sqrt{1+\left(\frac{\varepsilon''}{\varepsilon'}\right)^2} - 1\right]};$$
$$\beta = \omega\sqrt{\frac{\mu\varepsilon'\varepsilon_0}{2}\left[\sqrt{1+\left(\frac{\varepsilon''}{\varepsilon'}\right)^2} + 1\right]} \quad (5)$$

where $\omega = 2\pi f$ is the angular frequency; μ = magnetic permeability of soil; and ε' and ε'' = real and imaginary parts, respectively, of the relative dielectric constant. It is assumed that soils are nonmagnetic, and therefore the relative complex permeability of the soil is μ', where $\mu' = \mu/\mu_0$ and $\mu_0 = 1.257 \times 10^{-6}$ H/m. Hence, μ is 1.257×10^{-6} H/m.

The dielectric properties of soil are often estimated (Silva and Vuran 2010) using the following three equations:

$$\varepsilon = \varepsilon' - j\varepsilon'' \quad (6)$$

$$\varepsilon' = 1.15\left[1 + \frac{\rho_b}{\rho_s}\left(\varepsilon_s^{\alpha'} - 1\right) + \theta^{\beta'}\varepsilon_{f_w}'^{\alpha'} - \theta\right]^{1/\alpha'} - 0.68 \quad (7)$$

$$\varepsilon'' = [\theta^{\beta''}\varepsilon_{f_w}''^{\alpha'}]^{1/\alpha'} \quad (8)$$

where ε = relative complex dielectric constant of the soil-water mixture; θ = volumetric water content of the mixture; ρ_b = bulk density (g/cm^3); ρ_s = specific density of the solid soil particles; $\alpha' = 0.65$ = empirically determined constant; and ε_s = dielectric constant of soil particles, calculated as follows:

$$\varepsilon_s = (1.01 + 0.44\rho_s)^2 - 0.062 \quad (9)$$

The values of β' and β'' in Eqs. (7) and (8) are empirically determined constants, which are dependent on soil types (Peplinski et al. 1995); for instance

$$\beta' = 1.2748 - 0.519S - 0.152C;$$
$$\beta'' = 1.33797 - 0.603S - 0.166C \quad (10)$$

where S and C = mass fractions of sand and clay, respectively.

The real and imaginary parts of the relative dielectric constant of free water ε'_{f_w} and ε''_{f_w}, respectively, used in Eqs. (7) and (8), were computed by Peplinski et al. (1995) as follows:

$$\varepsilon'_{f_w} = \varepsilon_{w\infty} + \frac{\varepsilon_{w0} - \varepsilon_{w\infty}}{1 + (2\pi f \tau_w)^2} \quad (11)$$

$$\varepsilon''_{f_w} = \frac{2\pi f \tau_w (\varepsilon_{w0} - \varepsilon_{w\infty})}{1 + (2\pi f \tau_w)^2} + \frac{\sigma_{\text{eff}}}{2\pi\varepsilon_0 f}\frac{\rho_s - \rho_b}{\rho_s \theta} \quad (12)$$

where ε_{w0} = static dielectric constant of water (i.e., 80.1 at 20°C); $\varepsilon_{w\infty}$ = high-frequency limit of ε'_{f_w} (i.e., 4.9); τ_w = relaxation time of water (i.e., 9.23×10^{-12} s at 20°C); ε_0 = dielectric permittivity of free space (i.e., 8.85×10^{-12} F/m); and σ_{eff} = effective dielectric conductivity of soil, calculated as follows:

$$\sigma_{\text{eff}} = 0.0467 + 0.2204\rho_b - 0.4111S + 0.6614C \quad (13)$$

The preceding equations can be used to estimate the power loss of EM waves in soils with different volumetric water contents. Fig. 1 presents the results of such an evaluation for four different frequencies (170, 433, and 868 MHz, and 2.4 GHz). When the levels of a wireless system's transmission power, reception sensitivity, and antenna gains are all fixed, the penetration depth of the EM waves it emits and receives is directly related to the quantity of water in the soil and the operational frequency. In the case of the widely adopted license-free band of 2.4 GHz, the path loss is strongly influenced by the amount of water in the soil. Hence, the frequency of its EM wave is a key factor affecting how far a signal propagates through the soil (Akyildiz and Stuntebeck 2006; Akyildiz et al. 2009; Vuran and Silva 2010).

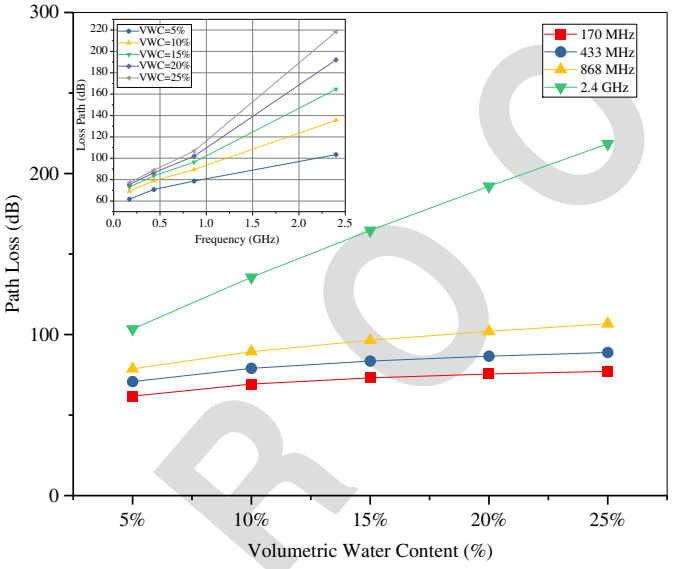

Fig. 1. VWC versus path loss at different frequencies.

Proposed Buried Wireless Sensor Network System

As shown in Fig. 1, sub-gigahertz wireless is worth exploring further in the sphere of B-WSN application. Hence, the B-WSN system proposed in the present paper was developed with a Texas Instruments (TI) (Dallas) high-performance sub-1-GHz transceiver (CC1120) that utilizes a low-power industrial/scientific/medical (ISM) band frequency of 433 MHz. The CC1120 transceiver is a fully integrated single-chip radio transceiver designed for high-performance and very-low-power wireless systems. The features of this transceiver are given in Table 1. This narrowband application (Lassen 2014)—defined as less than 25 kHz bandwidth—provides the optimum tradeoff between range and transmission time for ranges over 10 km and data rates of 1.2 kbps. Narrowband systems are characterized by excellent link budgets because narrow receiver filters remove most of the noise (Lassen 2014). Although narrowband WSN systems provide long-range radio-frequency (RF) communication in the air (more than 10 km), this study is the first to propose such a system for monitoring a full-scale buried pipeline exposed to earthquake-induced ground deformation.

Each node of the B-WSN consists of a microprocessor board, wireless module, and industrial D-cell battery (3.6 V, 19AHr), the wireless properties of which are provided in Table 2. The node was integrated with a frequency-domain reflectometry (FDR) sensor to enable it to monitor soil-moisture changes caused by pipe leakage. Wireless sensing nodes can work on multihop underground wireless topology, and the B-WSN system as deployed to support up to four hops. The maximum buried depth can archive 8 m with a single-hop penetration depth of more than 2 m. If set to take hourly readings and transmit them in real time, the nodes can operate for 2 years due to the system's ultra-low-power design for long battery life.

Evaluating Wireless Transmission Effectiveness of the B-WSN System in Soil

Experimental Setup

The proposed B-WSN's performance in underground EM propagation was first tested in a 0.5-m-diameter, 1.3-m-deep borehole.

Table 1. Main features of CC1120 wireless transceiver

Key parameter	Features
Sensitivity	−123 dBm at 1.2 kbps, −110 dBm at 50 kbps, and −127 dBm using built-in coding gain
Power supply	Wide supply voltage range (2.0–3.6 V)
Current consumption	2 mA in RX sniff mode, 17 mA peak current in low-power mode, and 22 mA peak current in high-performance mode
Data rates and modulation	Configurable data rates F0–200 kbps supported modulation formats: 2-FSK, 2-GFSK, 4-FSK, 4-GFSK, MSK, OOK
Peripherals and support functions	Enhanced wake-on-radio (eWOR), functionality for automatic low-power receive polling built-in coding gain support for increased range and robustness digital RSSI measurement temperature sensor

Note: RX = receive; FSK = frequency-shift keying; GFSK = Gaussian frequency shift keying; MSK = minimum-shift keying; and OOK = on-off keying.

Table 2. Wireless parameters of nodes

Parameter	Significant value
Operation frequency	433 MHz
Data rate	9.6 kbps
Antenna	1.5 dBi
Transmit power	26 dB
Receive sensitivity	−125 dBm
Battery capacity	19,000 mAH

Note: Multihop underground wireless topology; supports up to four hops.

Three wireless nodes were deployed in the experiment, as indicated in Fig. 2; and the experimental setup is shown in Fig. 3. Node 0, which acted as a gateway, was connected to a laptop and was responsible for data collection from the other two nodes. Node 1 was placed on the surface of the ground and Node 2 at the bottom of the hole. Node 1 served as a relay between Node 2 and Node 0 and was tasked with hopping the data, as shown in Fig. 4. The distance between Node 0 and Node 1 was 0.1 m. The borehole was sequentially filled with compacted soil at 0.2-m intervals, as shown in the right-hand diagram in Fig. 2. To facilitate measurement of the effect of burial on EM-wave propagation, the system's received signal strength index (RSSI) (in dBm) and its packet-loss values were recorded at every burial interval. The packet-loss rate represents data-reception quality and is calculated as the number of nonreceived packets divided by the number of packets sent; as such, a 0% rate indicates perfect reception and 100% indicates that no data packets were received during wireless communication.

Effects of Burial Depth

Prior to embedding Node 2 in the soil, the transmission performance between Nodes 1 and 2 through the air was examined. The resulting two way RSSI values were approximate −42 dBm (Node 2–Node 1) and −39 dBm (Node 1–Node 2). As the borehole was filled with soil in 0.2-m increments, the measured RSSI and packet-loss rates at the seven resulting burial depths were recorded (Table 3). The grading and volumetric water contents of the site soils retrieved at different depths are also provided in Table 3. There was no obvious correlation between packet-loss rate and burial depth, but RSSI decreased with increasing burial depth. The RSSI-21 (underground-to-surface) values were smaller than the RSSI-12 (surface-to-underground) values, indicating that the underground-to-surface transmission scenario was associated with more energy loss than its surface-to-underground counterpart. This result was to be expected, given that when an EM wave passes from a denser substance (e.g., soil) to a less-dense one (e.g., air), it is refracted away from the normal.

Fig. 5 shows the measured RSSI-21 values against burial depths as solid squares. Because the distance between Nodes 1 and 2 remained the same but the burial depths differed, the measured RSSI data are combinations of losses in the air and soil. The effect of air path loss was subtracted from the measured RSSI-21 after computation of the length of the air path using Eq. (1). The modified RSSI values, represented as solid circles in Fig. 5, were then plotted against burial depth, and the regression line yielded the following empirical equation:

$$\text{RSSI} = -56.456\,(\text{burial depth in meters}) + 0.765 \qquad (14)$$

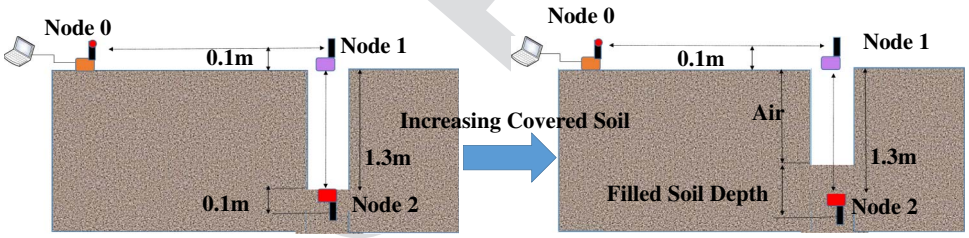

Fig. 2. Experimental schematic for evaluating signal strength at different soil depths.

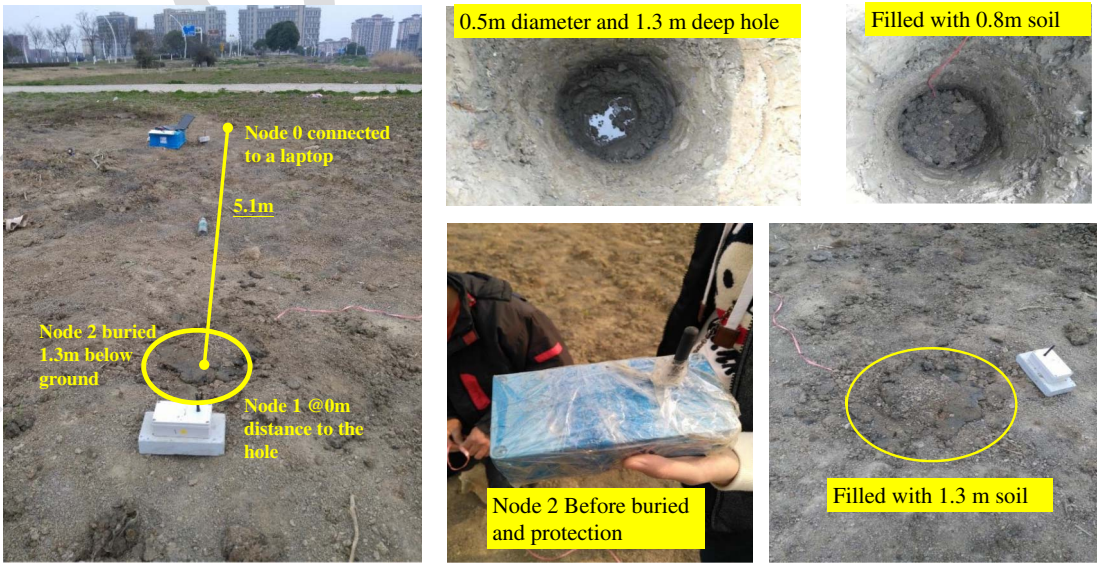

Fig. 3. Field experiment setup.

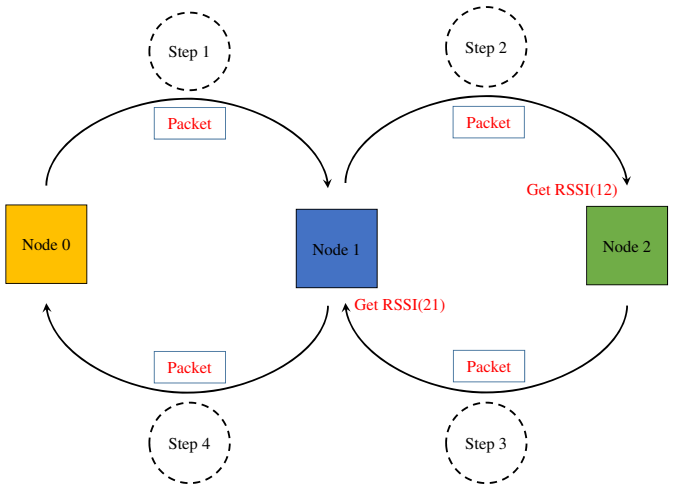

F4:1 **Fig. 4.** Data-meshing sequence.

If a radio link budget is 120 dB, a potential penetration of 2.13 m can be obtained from this regression.

Similar experiments using 433-MHz nodes were conducted in the past, mostly at 0.15- and 0.35-m burial depths, and the resulting data are also plotted in Fig. 5. Silva and Vuran's (2010b) experiment utilized a 433-MHz Mica2 mote with a maximum +10 dBm transmit power and obtained significantly different results from the present study for received signal strength at the same burial depth. In the case of a 0.35-m burial depth, RSSI increased by 68 dB when the transmission power was increased from +10 to +26 dBm. A similar study by Yu et al. (2017) examined various burial depths between 0 and 1 m using Crossbow's 433 MHz mote, again with maximum +10 dBm transmit power. Their findings, plotted as solid triangles in Fig. 5, closely match those of Silva and Vuran (2010b). Zaman et al. (2016) used the 433-MHz-based MoleNet platform to test the relationship between RSSI and burial depth, and their results are shown as dark gray triangles in Fig. 5. These are broadly similar to those of the present study in terms of their trends, but the RSSI they measured was lower, presumably because the maximum power of MoleNet is +13 dBm. Zemmour et al. (2017) utilized an Agilent 8722ES vector network analyzer (VNA)-based wireless system in 3.1–10.6 GHz ultrawideband band (UWB) with −9.9 to −14.3 dBm emitted power and a 3-dBi antenna to evaluate the performance of UWB in underground-to-surface communication. Probably because of their system's high-frequency input, the RSSI values they obtained at any given burial depth were small compared with the values measured by low-frequency systems.

Fig. 6 compares simulated and experimental path-loss results for different soil grades and volumetric water contents (VWCs). The path-loss values based on the experimental RSSI can be estimated as follows:

$$\text{Path loss} = T_x - R_x - 2\text{CBL} + 2\text{Ant\_Gain} \quad (15)$$

where R_x = received power; T_x = transmitting power; CBL = coaxial cable loss; and Ant_Gain = antenna gain.

Based on Eq. (15), the present study's experimental path-loss values have been plotted against burial depths, as marked by dark gray symbols in Fig. 6. In the same figure, diamonds and upside-down triangles represent the simulation-based path-loss values that were computed using the equations provided in the "Determining the Key Factors Affecting How Far a Signal Propagates through Soil" section, again plotted against burial depths. The sideways-facing triangle represents the path-loss values calculated using Eqs. (1)–(13) and the soil parameters listed in Table 3. The simulation results show that for a given soil grade, the higher the water content, the greater the path loss.

In Fig. 6, the simulation-based path-loss values of two different soils are represented by triangles (Simulation-VWC = 0.5, $S = 0.15$, and $C = 0.5$) and solid circles (Simulation-VWC = 0.5, $S = 0.5$, and $C = 0.15$). The simulation results show that for a given water content, the higher the mass fraction of clay, the greater the path loss becomes. The measured path-loss values (solid squares) in Fig. 6 are greater than those derived using the equations in the "Determining the Key Factors Affecting How Far a Signal Propagates through Soil" section and the soil parameters presented in Table 3. Because there are unlimited combinations to simulate the path loss, this variation in results reflects that the actual underground environment is heterogeneous. As such, the experimental results demonstrate the challenge of using simulations to predict path loss.

The proximity of the diamonds to the squares in Fig. 6 indicates that even though the water content (0.5) in the experimental case was lower than in the simulated case (0.8), the path-loss values were similar, showing that the use of experimental data to estimate the path loss and burial depth is conservative and practicable. This will necessitate the establishment of an experimental database based on testing on soils with differing water contents for the path loss–burial depth relationship, as shown in Fig. 6. On-site water-content measurement is a simple and inexpensive process.

Above-Ground Horizontal Transmission Distance for Different Burial Depths

For each different burial depth of Node 2, the position of Node 1 was moved horizontally along the ground surface until the RSSI-21 and RSSI-12 values were both less than −100 dBm. Each of these

Table 3. RSSI values and packet-loss rates for seven different soil depths with soil-sample particle analysis parameters

Soil depth (m)	VWC (%)	Soil-sample particle analysis parameters			Air distance (m)	RSSI		Packet-loss rate (%)
		Sand (%)	Silt (%)	Clay (%)		RSSI-21 (dBm)	RSSI-12 (dBm)	
0.1	33	3.4	72.4	24.2	1.4	−36	−32	4.16
0.3	33	1.6	76.2	22.2	1.2	−42	−37	2.41
0.5	33	1.6	76.2	22.2	1.0	−47	−42	1.86
0.7	52	1.2	79.2	19.6	0.8	−63	−57	0.00
0.9	52	1.2	79.2	19.6	0.6	−73	−66	0.82
1.1	55	0.7	78.5	20.8	0.4	−79	−72	16.98
1.4	55	0.7	78.5	20.8	0.1	−83	−77	1.63

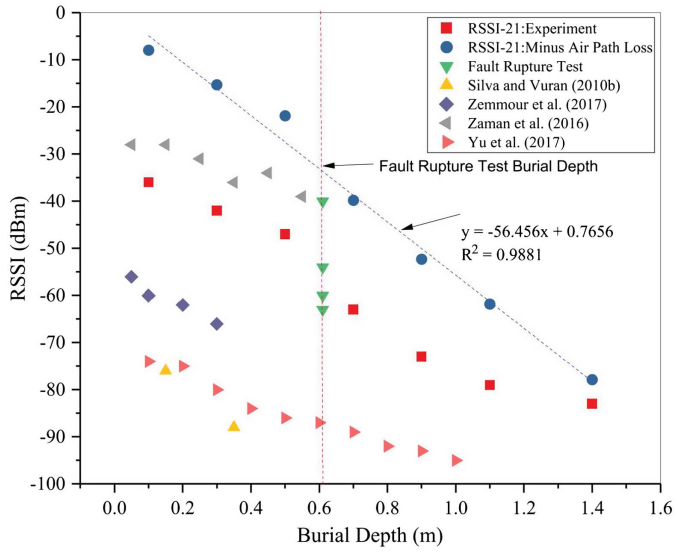

F5:1 **Fig. 5.** Analysis of RSSI by soil depth.

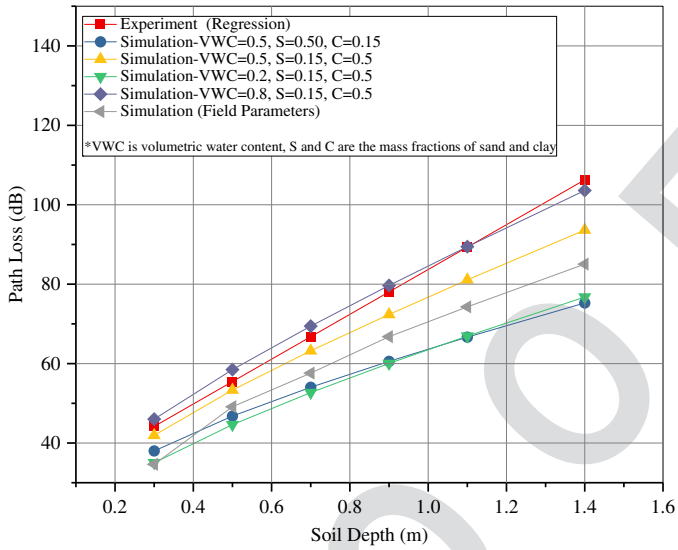

F6:1 **Fig. 6.** Comparison of experimental and simulated path-loss data.

limiting distances was recorded and, as shown in Fig. 7, increased as burial depth decreased. When Node 2 was completely buried 1.4 m below the surface of the ground, the maximal above-ground horizontal transmission distance was 1.5 m. At the same burial depth, the test was repeated with Node 1 positioned in all four of the cardinal compass directions from the borehole, but the effect of such changes in position on the EM waves' propagation characteristics was negligible.

Fig. 7 also shows that in Silva and Vuran's (2010a) system, burial depths of 0.15 and 0.35 m were associated with maximum receiving distances (defined as a 98% packet-loss rate) of 30 and 22 m, respectively. In the case of near-perfect transmission (1% packet-loss rate), Silva and Vuran's (2010a) horizontal transmission distances reduced to 25 and 20 m for the same two burial depths. Because of the transmission power difference discussed previously, the system proposed in the current paper achieved higher transmission distances than Silva and Vuran's (2010a) system.

Received Signal Strength Index versus Battery Voltage

The proposed B-WSN system is powered purely by its own internal industrial lithium thionyl chloride batteries. Special attention has been paid to the effects on RSSI values of declines in these batteries' voltage due to usage. During the indoor experiment, a receiver and transmitter were placed 50 cm apart on a table. The transmitter was powered by a direct current (DC) source, at settings ranging from 3.6 to 2.7 V, with the former simulating a new battery, and the latter an empty one. As shown in Fig. 8, there was a 7-dB difference for the transmit power. Therefore, careful circuitry redesign of the B-WSN nodes was critical so that the power supply to the radio chip could be maintained at a high and stable voltage that allowed for long-term radio communication. In practice, once a radio link was established, the transmission power was stable enough to ensure that it was maintained. Lithium thionyl chloride batteries were chosen because they supply a constant voltage when charged to anywhere between 10% and 100% of their capacity.

Investigating the Effectiveness of the B-WSN System for Monitoring Pipeline Joint Leakage Caused by Large Ground Movements

The findings of the field experiment described in preceding sections informed the design of a full-scale pipeline-rupture interaction experiment conducted at Cornell University. The burial depth of the model pipeline was 0.61 m, meaning that the RSSI required for the B-WSN system to operate effectively was estimated as −33.67 dBm based on the field experiment results. Considering the likely air and environmental path loss, the real RSSI was expected to be smaller than this estimation (Fig. 5). However, at this burial depth, it was expected that the wireless link quality of the newly developed B-WSN system would be acceptable. The system employed in the Cornell experiment consisted of wireless sensing nodes, gateway, remote server, and data-visualization software. Using the data shown in Fig. 7, the maximum horizontal distance from the buried sensing node to the gateway was estimated as 11 m. The wireless sensing nodes were buried near the pipeline to sense increases in moisture from pipe leakage caused by earthquake-induced movement. All the sensing data were sent to the gateway using a mesh network. The gateway uploaded data to the remote server either wirelessly, via 2G, 3G, or 4G network, or through an industry-standard RS232 connection that could be easily converted to standard services such as Wi-Fi, Ethernet, or fiber ports.

The full-scale rupture test was performed at Cornell University's Large-Scale Lifelines Testing Facility, which can be used to simulate fault rupture effects with as much as 1.8 m of strike-slip fault offset on pipelines as large as 600 mm in diameter. Full-scale rupture tests include detailed measurements of soil-pipeline interaction at various levels of rupture so that the performance of the pipeline system, including the pipe and its hazard-resistant joints, can be evaluated under actual failure conditions. Each test identifies both the pipeline's failure mechanism and the level of ground deformation that it can accommodate. The proposed B-WSN system was one of several advanced sensing devices that were tested simultaneously with this experiment.

Test Specimens and Instruments

Fig. 9 shows the test pipe and instruments in the test basin. The pipes used in this study were Bionax pipe and molecularly oriented polyvinyl chloride (PVCO) pipes with a nominal diameter of 150 mm, manufactured by IPEX (Montreal, QC, Canada). The outer pipe diameter and wall thicknesses were 175 and 6.2 mm,

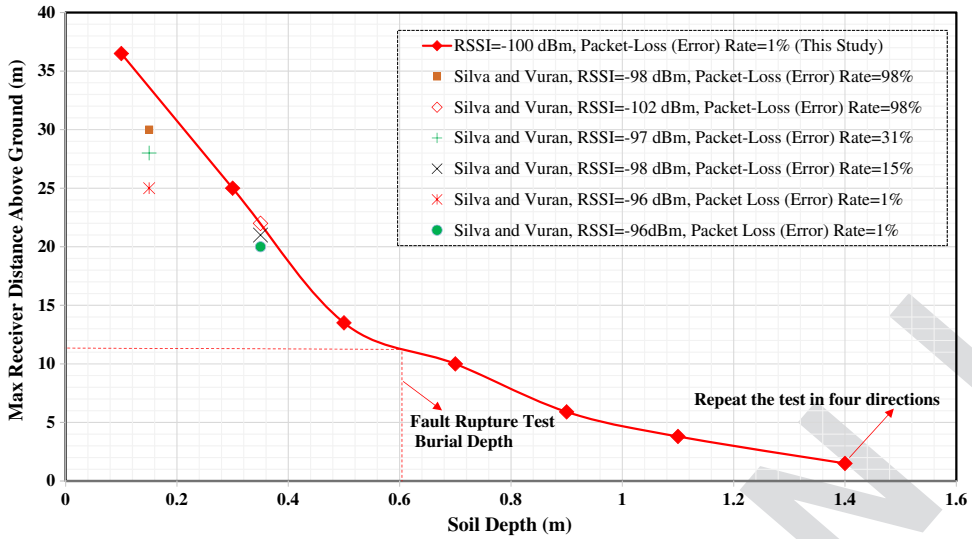

F7:1 **Fig. 7.** Maximum horizontal transmission distances for different burial depths.

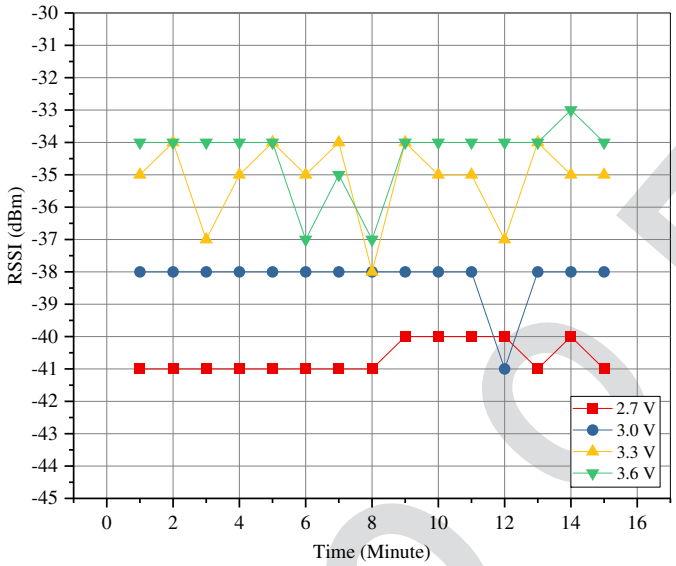

F8:1 **Fig. 8.** RSSI versus battery voltage.

respectively. The pipeline was composed of polyvinylchloride that had been manufactured to be molecularly oriented in the circumferential direction. Its two joints were C909 bell-and-spigot connections with extended bells and elastomeric gaskets fixed within each for watertight seals. The pipeline, which had an overall length of approximately 11.9 m, was fitted with commercially available Uni-FlangeVR pipe restraints (UFR1559-C-6-U style), manufactured by the Ford Meter Box (Wabash, Indiana). Four restraints, one on either side of each joint, were linked via six 15.8-mm threaded steel rods. The primary objective of the joint restraint was to increase the axial force capacity at the bell-and-spigot push-on joint after allowing the joint to displace axially to accommodate longitudinal deformation. Typical applications for such restraints include anchoring pressurization end caps and preventing the opening of unburied pipe joints during pressure checks (Wham et al. 2017b).

Fig. 10 illustrates the deployment layout of the IPEX pipe and wireless sensing nodes. The test specimen was buried in the Cornell large-scale test basin in partially saturated sand that was compacted to an average friction angle of 42°, equivalent in strength to that of a medium to dense granular backfill (O'Rourke 2010). The pipeline was placed on 0.2 m of soil, and the depth of burial to the top of the pipe was 0.81 m. A nominally 6-m-long pipe section was centered directly over the simulated fault line, with an intersection angle of 50°. The simulated fault rupture caused both tensile and bending strains in the pipeline. Two retaining walls were constructed inside the test basin to support the soil and allow access to the buried pipeline's end restraints, which provided fixed-end conditions.

As shown in Fig. 10, the main bodies of four wireless sensing nodes were each buried 0.2 m above the pipe and 0.61 m below the surface of the ground. One node was located next to each pipe joint to detect leakage when the pipeline ruptured, and the other two nodes were placed at a distance of 1.2 m away from the joints for reference purposes. Eight FDR soil-moisture sensors tasked with detecting water leakage and the pattern of its development were located below the pipe and connected in pairs to the four nodes by extension cables. The gateway was placed outside the test basin.

Alongside the B-WSN, various instruments were used to measure pipeline response. A total of 88 350-Ω foil gauges were installed at 17 locations along the specimen pipeline to measure axial and circumferential strains and evaluate axial forces and bending moments. Three string potentiometers were placed at each joint to measure the relative joint opening and joint rotation. These devices, along with other instruments, were protected from soil damage by telescopic shields fixed to the restraints. Lastly, four load cells were placed outside the pipe basin at each end to measure the axial force of reactions between the test basin's structural frame and the pipe end restraint. Throughout the test, the pipe was filled with water at an approximately constant pressure of 552 kPa. Additional descriptions of the test setup and instrumentation has been provided by Wham et al. (2017b).

Detecting Pipeline Joint Leakage Caused by Large Ground Movements

During the test, the southern part of the basin remained stationary while the northern section was displaced to the north and west by four large-stroke actuators to cause soil rupture and slippage at the interface between the basin's two parts. The soil rupture was representative of a left lateral strike-slip fault rupture, the most

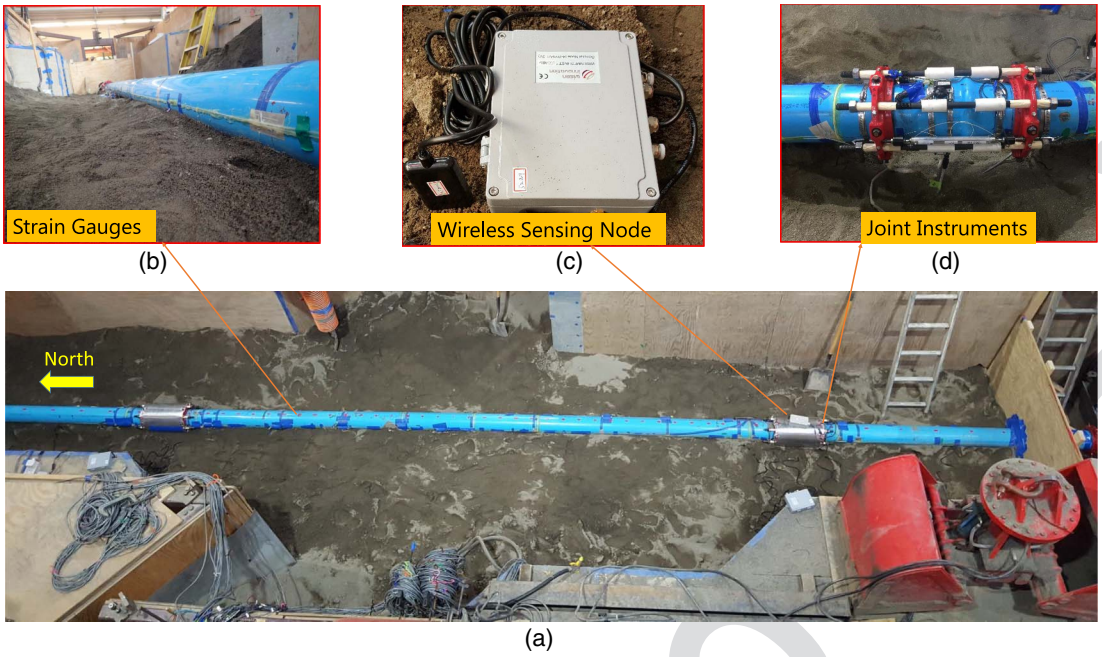

F9:1 **Fig. 9.** (a) IPEX pipe and instruments in the test basin; (b) strain gauges along the springline of the specimen; (c) wireless sensing node; and (d) joint
F9:2 instrumentation before shield attachment.

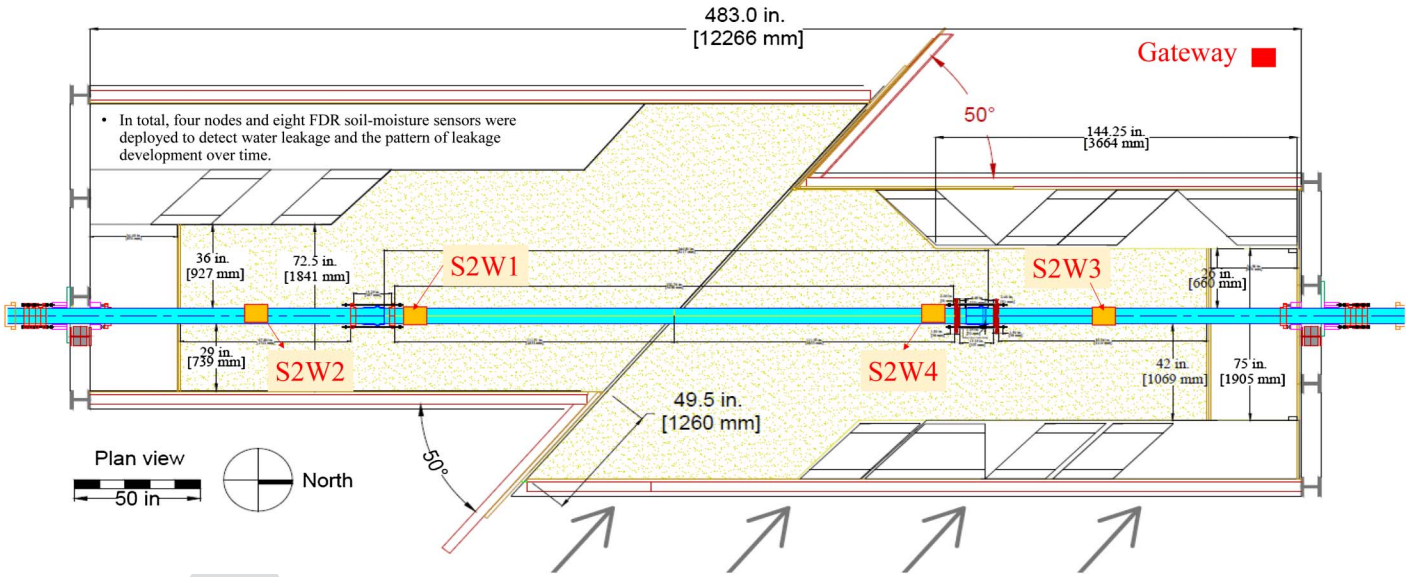

F10:1 **Fig. 10.** Plan view of IPEX pipe and wireless sensing nodes as deployed in the test basin.

severe ground deformation that occurs along the margins of liquefaction-induced lateral spreads and landslides.

Fig. 11(a) shows the surface of the test basin before the test commenced. Then, the north box was displaced at a rate of 50 mm/min. At 455 mm of fault displacement, an audible pop sound was heard, the pipeline depressurized, and the test was stopped [Fig. 11(b)]. Fig. 11(c) shows the deformed pipe as excavated following the test, along with breakage at its north joint. Fig. 11(d) is a close-up of the north joint showing the protective joint shield and pipe rupture.

Fig. 12 presents the proposed system's soil-moisture measurements alongside joint-opening, pipe-pressure, and fault-displacement data. Displacements of about 8.5 cm were measured at each joint just prior to a pipeline rupture. At a fault displacement of approximately 45 cm, i.e., when pipe failure occurred, all joint movements showed an abrupt jump in displacement due to elastic rebound. The northpass joint failure at its south restraint by circumferential rupture caused by the combination of elevated localized stress imposed by the restraint locking segments and the development of fault rupture–induced axial and bending strains along the pipe. The pipeline reached strain levels near 1% prior to failure, and the response was consistent with performance observed during preliminary tension and bending tests (Wham et al. 2017a, b).

Each movement of the basin caused the pipe to increase slightly in overall length, which in turn caused its initial pressure of 552 kPa to fluctuate slightly, as shown in Fig. 12. At a fault displacement of

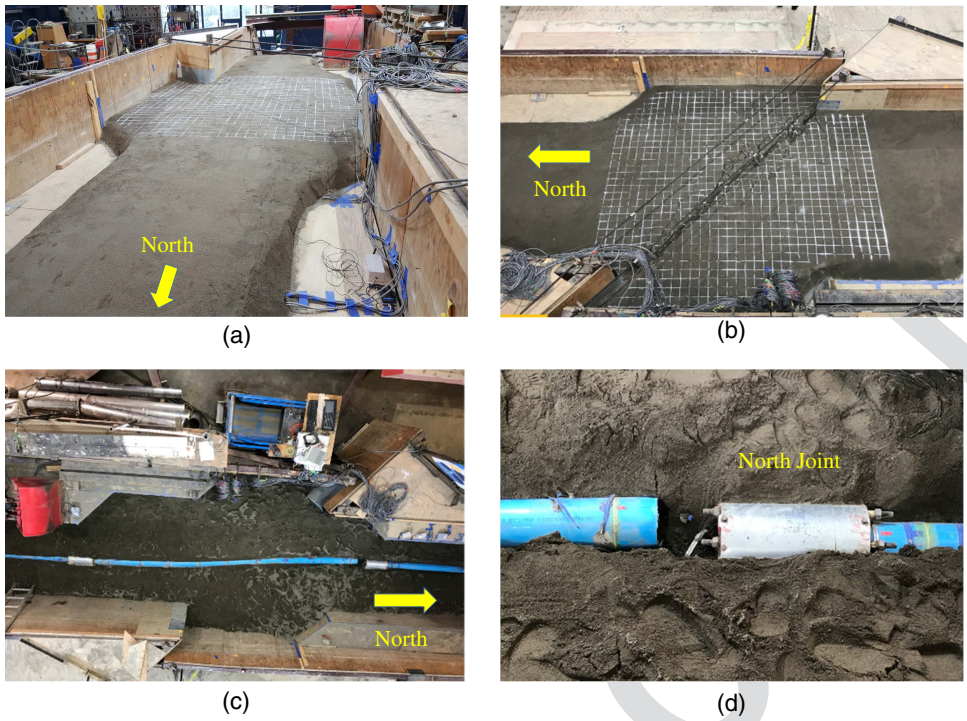

F11:1 F11:2 **Fig. 11.** (a) Test basin before test; (b) position of test basin at the moment of pipe failure; (c) pipe as excavated following the test; and (d) damage to pipe at north joint.

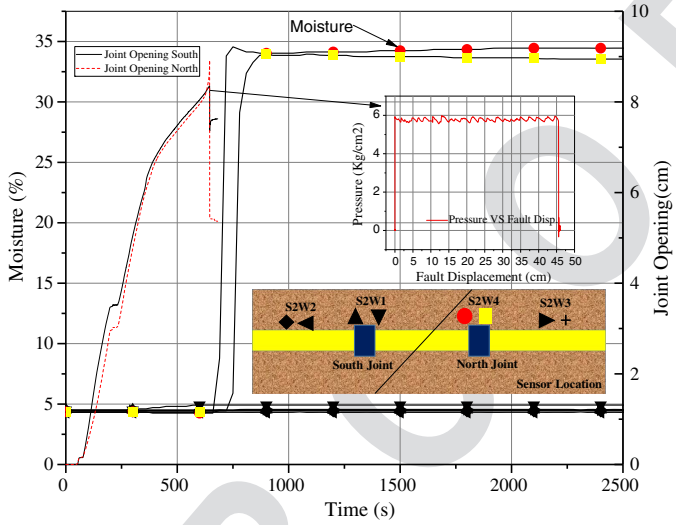

F12:1 F12:2 **Fig. 12.** Soil-moisture plotted against joint-opening, pipe-pressure, and fault-displacement data.

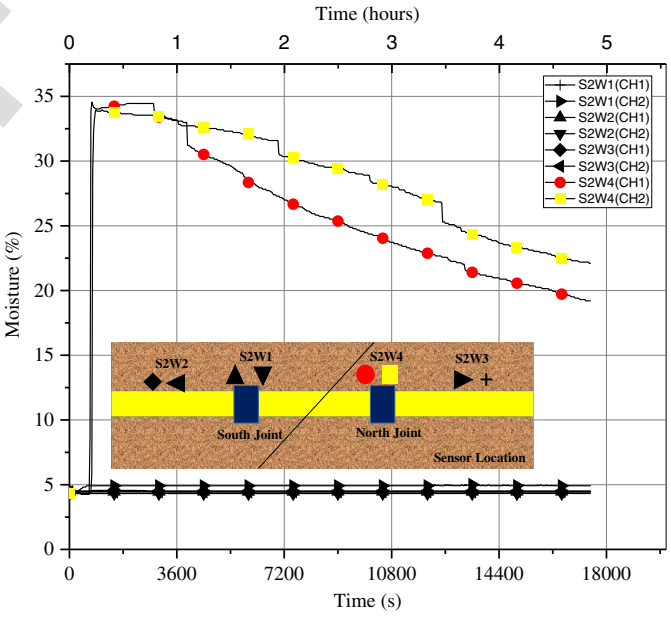

Fig. 13. Long-term trend of soil moisture after leakage. F13:1

roughly 0.45 m, there was a sudden loss of pressure in the pipe, indicating pipe rupture and leakage. Fig. 12 demonstrates how the wireless sensing nodes with soil-moisture sensors performed in identifying the leakage location. Specifically, upon the sudden loss of pressure in the pipe, the moisture value registered by the sensing node at the north joint (S2W4) increased to approximately 35% moisture, whereas the mean of the moisture values registered by the other three nodes remained at around 4.5% moisture.

Fig. 13 presents the long-term trend of soil moisture measurements at the leak location. The recorded moisture remained high during the first hour following the test, and then gradually reduced to 20%–22% moisture over the next 4 h.

In this experiment, the sensing nodes were able to transmit data to the gateway via just one hop. Fig. 14 presents a comparison of RSSI before and after the experiment, which reveals that pretest RSSI variation was small. During the experiment, however, the RSSI experienced a significant variation of up to 20–25 dB due to various factors including node movement, movement of people, and mechanical effects. Moreover, RSSI variation was more apparent in S2W1 and S2W2, which were located farther from the gateway than the other two nodes, and thus were subject to greater multipath reflection and refraction. At the same burial depth as

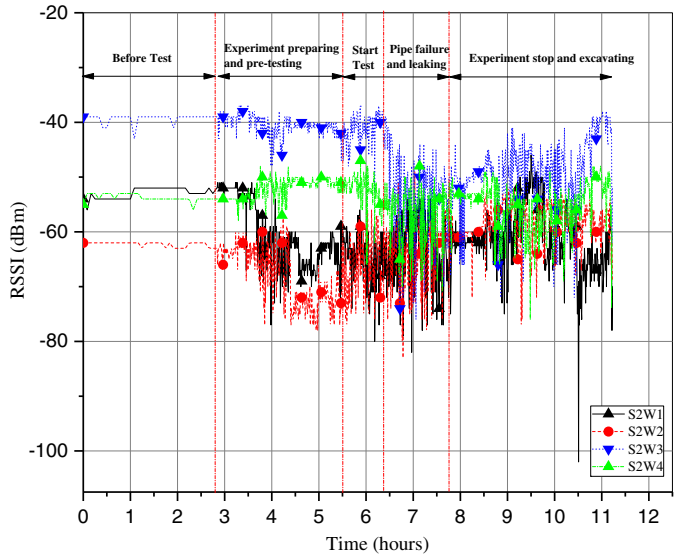

F14:1 **Fig. 14.** RSSI before, during, and after the test.

the model pipeline in the Cornell experiment, i.e., 0.61 m, the RSSI estimate based on the field experiment (Fig. 5) was −33.67 dBm. This most closely approximated the performance of node S2W3 in the Cornell experiment, i.e., −40 dBm. As shown in Fig. 7, the maximum horizontal distance from any node to the gateway was around 11 m. The RSSI of the farthest node from the gateway, S2W2, was −61 dBm before the test and −79 dBm during it. Because the receiver sensitivity of the proposed B-WSN is −125 dBm, these figures indicate that such a system is sufficient for regular communication during the magnitude and type of event simulated by the experiment.

Discussion and Conclusions

Previous studies have not reported on the efficiency with which B-WSNs can detect joint leakage caused by large ground movement, and few researchers have addressed the behavior of B-WSNs during severe ground deformation. One of the primary goals of this study was therefore to develop and investigate the effectiveness of B-WSN-based monitoring of pipeline joint leakage caused by large ground movements. The results of simulations indicated that the developed sub-gigahertz wireless system is worth exploring further in the sphere of B-WSN applications. Field-experiment data successfully estimated the path loss and burial depth that would emerge from the full-scale rupture test. The results showed the potential for B-WSNs to be employed to detect joint leakage, and that the proposed B-WSN could help considerably in diagnosing damage to buried pipes before they are excavated.

This paper has discussed the development and performance testing of a B-WSN system for detecting pipeline leakage for a system with 26 dB transmit power, −125 dBm sensitivity, and a 1.5-dBi omnidirectional antenna. The maximum burial depth of this system is 1.4 m greater than the experimental results in the previous literature (Silva and Vuran 2010a, b; Yu et al. 2017; Zaman et al. 2016; Zemmour et al. 2017). When buried at 35 cm, the system's RSSI was higher by 68 dB than similar prior systems (Silva and Vuran 2010; Yu et al. 2017) with lower transmission power, i.e., +10 dBm compared with the present system's +26 dBm. Likewise, penetration depth increased from 0.2 to 1.4 m when RSSI was −75 dBm. The present study's preliminary results indicated that the benefits of increasing transmission power were likely to include increases to penetration depth, and accordingly, applied an experimental approach to the estimation of burial depth.

The full-scale rupture test results verified that the B-WSN system could conclusively identify the location and pattern of water leakage from a pipeline that fails due to severe ground deformation as soon as 1 min after the pipeline has failed. The experiment has provided evidence that real-time leakage detection is possible using a low-latency wireless system. The findings also identified a long-term trend in soil moisture change after a pipeline failure occurs and exemplify how the B-WSN system may be useful for pipeline performance testing under large ground deformation (Wham et al. 2017a, b).

Regarding path-loss performance, the experimental data are broadly in agreement with the predictions made. The average packet-loss rate was less than 0.1% during the experiment. The sensing nodes were able to transmit data to the gateway with only one hop, and the average power consumption of each sensing node was 26.5 mA per 30 s sampling/wireless-communication period. Thus, the sensing nodes can be expected to function for 27 days if powered by four D-cell batteries. If the sampling interval were changed to an hour, however, each sensing node would work for 2 years or more.

The results reported in this paper indicate that the newly developed B-WSN system has considerable promise for real-world pipeline-monitoring applications. Firstly, the results have shown that the B-WSN can penetrate at least 1.4 m of soil; and coupled with the radio-link budget of 120 dB, an analytical penetration of 2.13 m can be obtained. Its wireless sensing nodes can work on multihop underground wireless topology, and the system as deployed was designed to support up to four hops. Consequently, its maximum practical burial depth is 8 m, based on a single-hop penetration depth of more than 2 m, making it a workable option for most shallowly buried pipelines. Secondly, the B-WSN can be deployed more quickly and in larger quantities than wired sensing systems. In the conducted experiment, only 1 h elapsed between the beginning of system installation and the appearance of the first live data online. Thirdly, the B-WSN has demonstrated its potential value for pipeline management. For example, the underground wireless nodes can locate possible pipeline faults, and the system saves all such information permanently in the cloud for the pipeline operator to use when repairing and replacing pipes. Uniquely, during excavation, the RSSI of the B-WSN system can be used to judge the buried depth of the pipeline to avoid damage to it.

The target of this study was for monitoring water supply networks, but further investigation may show that the proposed system can be adapted for other buried systems such as wastewater pipelines. Although FDR sensors were used in this study, they can be replaced with other sensors depending on specific sensing applications.

Acknowledgments

The authors would like to thank the Ministry of Science and Technology of the Republic of China, Taiwan, and Sinotech Engineering Consultants for financially supporting (ID: 105-2917-I-564 -053) this research. The authors are also grateful to Cornell University for supporting the Large-Scale Lifelines Testing Facility, and to Jitong Sun, Xiaoyan Huang, and Fei Du for their site work and technical support for B-WSN.

References

Akyildiz, I. F., and E. P. Stuntebeck. 2006. "Wireless underground sensor networks: Research challenges." *Ad Hoc Networks* 4 (6): 669–686. https://doi.org/10.1016/j.adhoc.2006.04.003.

Akyildiz, I. F., Z. Sun, and M. C. Vuran. 2009. "Signal propagation techniques for wireless underground communication networks." *Phys. Commun.* 2 (3): 167–183. https://doi.org/10.1016/j.phycom.2009.03.004.

Ali, S., S. B. Qaisar, H. Saeed, M. F. Khan, M. Naeem, and A. Anpalagan. 2015. "Network challenges for cyber physical systems with tiny wireless devices: A case study on reliable pipeline condition monitoring." *Sensors* 15 (4): 7172–7205. https://doi.org/10.3390/s150407172.

Almazyad, A. S., Y. M. Seddiq, A. M. Alotaibi, A. Y. Al-Nasheri, M. S. BenSaleh, A. M. Obeid, and S. M. Qasim. 2014. "A proposed scalable design and simulation of wireless sensor network-based long-distance water pipeline leakage monitoring system." *Sensors* 14 (2): 3557–3577. https://doi.org/10.3390/s140203557.

Jawhar, I., N. Mohamed, M. M. Mohamed, and J. Aziz. 2008. "A routing protocol and addressing scheme for oil, gas, and water pipeline monitoring using wireless sensor networks." In *Proc., 5th IFIP Int. Conf. on Wireless and Optical Communications Networks*, 1–5. New York: IEEE.

Jawhar, I., N. Mohamed, and K. Shuaib. 2007. "A framework for pipeline infrastructure monitoring using wireless sensor networks." In *Proc., Wireless Telecommunications Symp.*, 1–7. New York: IEEE.

Lai, T. T.-T., W.-J. Chen, K.-H. Li, P. Huang, and H.-H. Chu. 2012. "Triopusnet: Automating wireless sensor network deployment and replacement in pipeline monitoring." In *Proc., 11th Int. Conf. on Information Processing in Sensor Networks*, 61–72. New York: ACM.

Lassen, T. 2014. *Long-range RF communication: Why narrowband is the de facto standard*. White Paper. Dallas: Texas Instruments.

O'Rourke, T. 2010. "Geohazards and large, geographically distributed systems." *Géotechnique* 60 (7): 505–543. https://doi.org/10.1680/geot.2010.60.7.505.

Peplinski, N. R., F. T. Ulaby, and M. C. Dobson. 1995. "Dielectric properties of soils in the 0.3–1.3 GHz range." *IEEE Trans. Geosci. Remote Sens.* 33 (3): 803–807. https://doi.org/10.1109/36.387598.

Silva, A. R., and M. C. Vuran. 2010a. "Communication with aboveground devices in wireless underground sensor networks: An empirical study." In *Proc., IEEE Int. Conf. on Communications*, 1–6. New York: IEEE.

Silva, A. R., and M. C. Vuran. 2010b. "Development of a testbed for wireless underground sensor networks." *EURASIP J. Wireless Commun. Networking* 2010: 1–14.

Stoianov, I., L. Nachman, S. Madden, T. Tokmouline, and M. Csail. 2007. "PIPENET: A wireless sensor network for pipeline monitoring." In *Proc., 6th Int. Symp. on Information Processing in Sensor Networks*, 264–273. New York: IEEE.

Sun, Z., P. Wang, M. C. Vuran, M. A. Al-Rodhaan, A. M. Al-Dhelaan, and I. F. Akyildiz. 2011. "MISE-PIPE: Magnetic induction-based wireless sensor networks for underground pipeline monitoring." *Ad Hoc Networks* 9 (3): 218–227. https://doi.org/10.1016/j.adhoc.2010.10.006.

Tan, X., Z. Sun, and I. F. Akyildiz. 2015. "A testbed of magnetic induction-based communication system for underground applications." *IEEE Antennas Propag. Mag.* 57 (4): 74–87.

Vuran, M. C., and A. R. Silva. 2010. "Communication through soil in wireless underground sensor networks–Theory and practice." In *Sensor networks*, 309–347. Berlin: Springer.

Wham, B. P., C. Argyrou, T. D. O'Rourke, H. E. Stewart, and T. K. Bond. 2017a. "PVCO pipeline performance under large ground deformation." *J. Pressure Vessel Technol.* 139 (1): 011702. https://doi.org/10.1115/1.4033939.

Wham, B. P., B. Berger, T. O'Rourke, C. Payiya-Ekkasut, and H. Stewart. 2017b. *Performance evaluation of Bionax SR PVCO pipeline with extended bell joints under earthquake-induced ground deformation*. Ithaca, NY: Cornell Univ.

Yu, H., and M. Guo. 2012. "An efficient oil and gas pipeline monitoring systems based on wireless sensor networks." In *Proc., Int. Conf. on Information Security and Intelligence Control*, 178–181. New York: IEEE.

Yu, X., Z. Zhang, and W. Han. 2017. "Evaluation of communication in wireless underground sensor networks." In *Proc., IOP Conf. Series: Earth and Environmental Science*, 012083. Bristol, England: IOP Publishing.

Zaman, I., M. Gellhaar, J. Dede, H. Koehler, and A. Foerster. 2016. "Design and evaluation of MoleNet for wireless underground sensor networks." In *Proc., IEEE 41st Conf. on Local Computer Networks Workshops*, 145–147. New York: IEEE.

Zemmour, H., G. Baudoin, and A. Diet. 2017. "Soil effects on the underground-to-aboveground communication link in ultrawideband wireless underground sensor networks." *IEEE Antennas Wirel. Propag. Lett.* 16: 218–221. https://doi.org/10.1109/LAWP.2016.2570298.

Queries

1. Please check and confirm whether all affiliations are set correctly.
2. Please check and confirm whether that all the corrections are incorporated correctlty.
3. Please clarify whether the reference citation “Silva and Vuran 2010a” or “Silva and Vuran 2010b” to be cite haere.
4. Please check and confirm edits made in footnote of Table 2.
5. Please clarify whether the reference citation “Silva and Vuran 2010a” or “Silva and Vuran 2010b” to be cite haere.